Axially equilibrated displacement-based fibre beam element for bidirectional response modelling

F. Cavalieri[1], M. Calò[2], J.P. Almeida[3] and R. Pinho[4]

ABSTRACT: Although distributed plasticity beam elements include formulations that verify a strict equilibrium of the axial forces along the element length, known as force-based (FB) approaches, the classical conventional displacement-based (DB) elements show advantages in simulating the response of some structural members. However, the latter do not verify strong equilibrium of the axial forces, but only the weak or integral form of equilibrium. To fix this issue, several authors recently proposed enhanced strain formulations that respect a strict equilibrium along the axial direction, obtained through iterations on the cross-sectional average strain in each section. Unfortunately, most research efforts on innovative beam formulations have been directed towards planar (2D) elements, instead of spatial (or 3D) formulations. This work thus presents the implementation of a 3D axially equilibrated DB (DB/ae) beam element in the finite element software OpenSees, as an enhancement of the classical displacement-based (DB/c) formulation. In order to present advantages and drawbacks of the proposed 3D DB/ae beam element, its numerical responses are compared with those obtained from the DB/c and FB elements, first with reference to an application example featuring bidirectional loading, and then taking the experimental data from one series of quasi-static bidirectional cyclic tests, related to two reinforced concrete (RC) thin walls, as benchmark.

1 INTRODUCTION

The accurate simulation of the nonlinear bidirectional behaviour of vertical members, namely columns and walls, together with the influence of variation of the axial force, is assuming growing importance. However, given that nonlinear analyses of entire structures are computationally time consuming, engineers and researchers are usually forced to resort to the use of beam elements. Unfortunately, the ability of beam elements to simulate the bidirectional response of members is still unsatisfactory, for which two main reasons contribute: on the one hand, the overall paucity of high-quality experimental results; on the other, the insufficient development and validation of beam finite elements. Both aspects are briefly revised below for reinforced concrete (RC) structures.

Experimental research on the inelastic response of RC members under compressive axial force and biaxial lateral cyclic loading is still limited, when compared to one-dimensional loading. It has been known for long that cyclic biaxial bending demands on RC columns tend to reduce their capacity and cause stiffness and strength deterioration during successive load reversals (Takizawa and Aoyama, 1976). A number of test programmes have followed, in which unfortunately not all experimental information required for model development and calibration has been measured or reported. The test programmes continued in this century (e.g. Rodrigues *et al.*, 2013; Raza *et al.*, 2020),

[1] *Dr., European Centre for Training and Research in Earthquake Engineering (EUCENTRE), Via Adolfo Ferrata 1, 27100 Pavia, Italy, e-mail address: francesco.cavalieri@eucentre.it*
[2] *Mr., Department of Civil Engineering and Architecture, University of Pavia, Via Adolfo Ferrata 5, 27100 Pavia, Italy, e-mail address: mattia.calo@unipv.it*
[3] *Dr., Institute of Mechanics, Materials and Civil Engineering (IMMC), Civil and Environmental Engineering, École Polytechnique de Louvain, GCE Place du Levant 1/L5.05.01 1348 Louvain-la-Neuve, Louvain, Belgium, e-mail address: joao.almeida@uclouvain.be*
[4] *Prof., Department of Civil Engineering and Architecture, University of Pavia, Via Adolfo Ferrata 5, 27100 Pavia, Italy, e-mail address: rui.pinho@unipv.it*

and revealed significant coupling among the three loading directions, showing that damage in one direction reduces stiffness in the other. Over the last couple of decades, bidirectional tests have also been performed by several researchers (e.g. Almeida *et al.,* 2017) on RC walls featuring cross-sections of different geometries. The influence of bidirectional loading in the response is clear, reducing in general the displacement capacity with respect to unidirectional loading.

Simulating numerically with beam elements the wide range of members and bidirectional effects is often addressed by employing distributed plasticity formulations, the latter being naturally associated with cross-sectional fibre discretisation. Although the force-based (FB) formulation verifies a strict equilibrium of the axial forces along the element length, the classical conventional displacement-based (DB) elements show some advantages in simulating resisting mechanisms in structural members such as tension shift, which tend to cause a linear curvature profile. However, DB elements do not strictly equalise equilibrium of the axial forces along the element with the imposed axial loads, and only the finite element weak form is verified. To fix this issue, several researchers, among which Tarquini *et al.* (2017), proposed enhanced strain formulations that respect a strict equilibrium along the axial direction, obtained through iterations on the cross-sectional average strain in each section. Unfortunately, such research efforts on innovative beam formulations were directed towards planar (2D) elements, instead of 3D formulations. Based on the axially equilibrated DB (DB/ae) formulation proposed by Tarquini *et al.* (2017) for the planar case and its extension to 3D carried out by Cavalieri *et al.* (2022), the contribution given by the present work is the implementation of such a spatial DB/ae beam element in the finite element software OpenSees (McKenna *et al.*, 2000), as an enhancement of the classical displacement-based (DB/c) formulation. The numerical performance of the newly implemented element was herein compared with those obtained with the classical (DB/c and FB) elements so as to highlight their relative advantages and drawbacks, firstly considering an example column subjected to monotonic and cyclic bidirectional loading, and then using experimental results from quasi-static bidirectional cyclic tests on two RC thin walls as benchmark.

2 PERFORMANCE AND FEATURES OF THE 3D DB/AE ELEMENT

This section illustrates the features of the developed 3D axially equilibrated DB (DB/ae) beam (Cavalieri *et al.*, 2022) element under idealised monotonic and cyclic loadings, exploiting the bidirectional response of simple structures. The element was implemented in the finite element software OpenSees, as an enhancement of the classical displacement-based (DB/c) formulation. The input parameters to be defined are the same required by the 2D version of the axially equilibrated DB element, developed by Tarquini *et al.* (2017), plus the torsional rigidity, *GJ.* Such input parameters are also the same required by the classical DB element in OpenSees, except for the axial force tolerance, which must be explicitly defined in the DB/ae case. The latter tolerance expresses the maximum axial force unbalance accepted between the integration points (IPs).

In this section, the main features of the proposed DB/ae element are presented and compared with those of the DB/c and force-based (FB) elements at the global level, in order to highlight their relative advantages and drawbacks, with reference to an application example extended to bidirectional loading. The latter, already used in Tarquini *et al.* (2017), consists of a three-metre length RC cantilever column, subjected to an axial load of 60 kN, corresponding to an axial load ratio of about 1.2%, and imposed lateral displacements at the free end, Δ_x and Δ_y, along the two horizontal directions, x and y. The RC section has dimensions of 300 × 400 mm^2, with a concrete cover of 20 mm in both directions. The longitudinal reinforcement is composed of 12 ϕ16 mm steel bars, corresponding to a reinforcement ratio of about 2%. A schematic representation of the column and its sectional properties are shown in Figure 1.

The column model was discretised with two equal-length finite elements for the DB formulations (i.e. DB/ae and DB/c), and only one element for the FB formulation. Each element was assigned four Gauss-Lobatto integration sections. Regarding the sectional discretisation, twelve fibres in both directions were used to discretise the concrete core, eight by two fibres were adopted for the concrete cover at both sides (parallel to the *x*- and *y*-directions), whereas the longitudinal reinforcing bars were modelled with one fibre each. Geometric nonlinearities were not included (i.e. a linear geometric transformation was used). The constitutive relationship proposed by Popovics (1973), implemented in the Concrete04 material model in OpenSees, was used for both confined and unconfined concrete, with the values reported in Table 1 for the following parameters: Young's modulus E_c, unconfined concrete compressive strength f'_c, unconfined concrete strain at maximum strength ε_c, confined concrete compressive strength f'_{cc}, confined concrete strain at maximum strength ε_{cc}. On the other hand, the Menegotto-Pinto (1973) constitutive law, represented by the Steel02 material model in OpenSees, was assigned to the longitudinal reinforcement, with the values reported in Table 1 for the following parameters: Young's modulus E_s, yield strength f_y, strain-hardening ratio b. Given these material and sectional properties, the torsional rigidity resulted to be GJ = 22429 kNm^2.

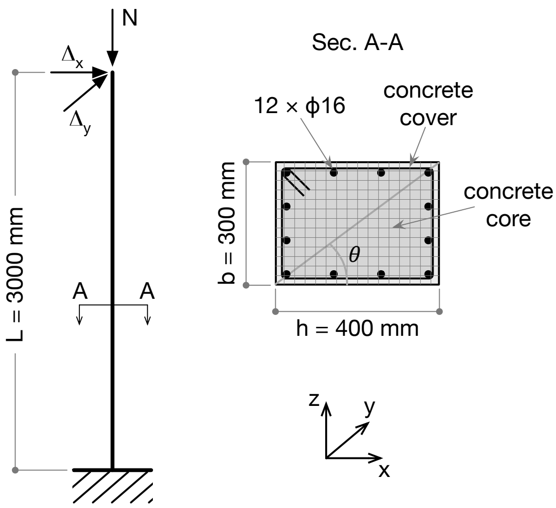

Figure 1. Application example: structural representation and sectional properties.

Table 1. Parameter values adopted for concrete and steel in the application example.

E_c (GPa)	f'_c (MPa)	ε_c (‰)	f'_{cc} (MPa)	ε_{cc} (‰)	E_s (GPa)	f_y (MPa)	b (‰)
30	37	2	42	3	200	480	5

2.1 Monotonic loading

The first exercise carried out to present the main features of the implemented 3D DB/ae formulation consisted in modelling the column with both the 2D and 3D versions of the DB/ae formulation, adopting the element discretisation for the DB formulations described above, and applying a monotonic loading in displacement control along the *x*-direction at the column's free end. The aim herein was to prove that the 3D DB/ae element, when used in a 2D loading scheme, provides the same results as its 2D version: this is in fact what was observed, with the two shear force-displacement curves appearing to be superimposed, thus reassuring on this first important requirement of the implemented element.

Subsequently, three column models were created using the three formulations at hand (i.e. DB/ae, DB/c and FB), and a monotonic bidirectional loading was applied in displacement control at the free end of the column along the section diagonal. It is worth noting that two components of incremental load, equal to cos(θ) and sin(θ), where θ is the angle defining the direction of the section diagonal with respect to the *x*-axis (see

Figure 1), were applied along the *x*- and *y*-directions, respectively. However, since the displacement control within a pushover analysis in OpenSees can only be enforced along one direction, which was herein selected to be the *x*-direction, the target displacement of 0.4 m was reached along the *x*-direction only (see Figure 2a), whilst a non-monitored maximum displacement was attained along the *y*-direction.
The resulting shear-displacement curves, for both horizontal directions, are displayed in Figure 2a) and Figure 2b). The largest force capacity is unsurprisingly provided by the DB/c formulation, owing to the constraints imposed in both the axial and transversal displacement fields. By imposing axial equilibrium, and thus removing the axial strain constraint, the model using the DB/ae formulation exhibits a reduction in the simulated shear in both directions. The weakest response is provided by the FB formulation, where no displacement fields are assigned and exact equilibrium is satisfied. This global behaviour is expected and consistent with what observed by Tarquini *et al.* (2017) for the 2D version of the DB/ae formulation, thus further reassuring on the accuracy of the 3D implementation carried out in this work.

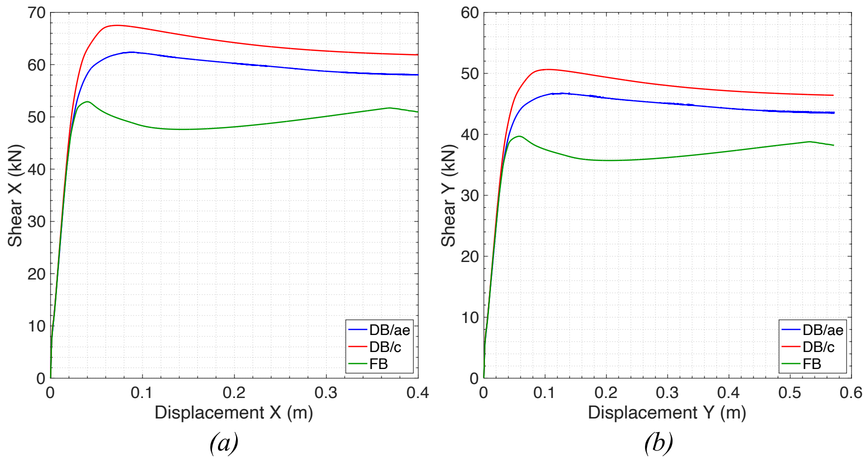

Figure 2. Shear-displacement curves for the DB/ae, DB/c and FB formulations, in the (a) x-direction and (b) y-direction, when a monotonic loading is applied along the cross-section diagonal.

With reference to these pushover results, the numerical performance of the 3D DB/ae formulation was compared with that of the other two formulations, finding that computational time increased by a factor of around three with respect to the classical DB and FB formulations. This is due to the additional axial-equilibrium iterative level and it obviously depends, as discussed in the previous section, on the specified tolerance; the latter was set to 10^{-5} N, a quite stringent value, for all the simulations carried out in this work. However, the increased computational cost required by the proposed 3D DB/ae formulation also entails important advantages, especially with respect to the DB/c formulation and at the local level, as it will be shown in the next subsection with reference to axial force estimation, as well as in the comparison against experimental testing results in Section 3.

2.2 Cyclic loading: loading along the cross-section diagonal and clover leaf pattern

For the column models implementing the three formulations, the analysis was then extended to bidirectional cyclic loading. In the first example, the simple cyclic displacement pattern with three cycles shown in Figure 3a,top) was applied at the free end of the column along the section diagonal. The same scheme, applied previously, of two components of incremental loading and displacement control along the *x*-direction only, was also adopted in this case. Figure 3b,top) shows the axial force values obtained with the DB/ae and DB/c formulations at the four IPs of the base element. The curves related to the different IPs are superimposed and shown with the same colour, for each of the two DB formulations. The plot clearly confirms what was expected, that is, the use of classical displacement-based elements ensures axial equilibrium only in an average sense and yields different values of axial force at distinct IPs, whilst the 3D DB/ae formulation leads the axial force in the four IPs to be constant and practically coincident with the external applied axial load. The resulting shear force-displacement curves, for both horizontal directions, are displayed in Figure 3a,bottom) and Figure 3b,bottom). The same relationships between the elements in terms of lateral strength response, already observed for the monotonic loading case above (Figure 2), also apply to this case: at the global level, the behaviour of the DB/ae element appears to be intermediate between the ones of the other two elements, showing a stable numerical performance.

In the second example, a more complex bidirectional displacement pattern, following a clover leaf shape, was applied at the free end of the column. Contrarily to the previous cases, where displacement could be controlled along one direction only, this example required to apply target displacements in both horizontal directions. To the authors' knowledge, the only analysis type in OpenSees that allows imposing a target action (force, displacement, acceleration) along several directions at the same time is dynamic analysis. In undertaking the latter, the displacement pattern shown in the bottom-left corner of Figure 4b) was applied using two single-point constraints (*sp* command in OpenSees), one per horizontal direction. Naturally, the model was assigned no mass and damping, so as to avoid giving rise to inertial and damping forces. The responses of the DB/ae, DB/c and FB formulations were compared at the global level, in terms of shear-displacement curves in both horizontal directions and shear-shear curve, as shown in Figure 4. The same intermediate response of the DB/ae element is again observed in this case, thus confirming the reliability of the proposed formulation in handling material nonlinearities in a bidirectional static loading scheme. These two examples illustrate the stability of the proposed formulation and its correct implementation in OpenSees.

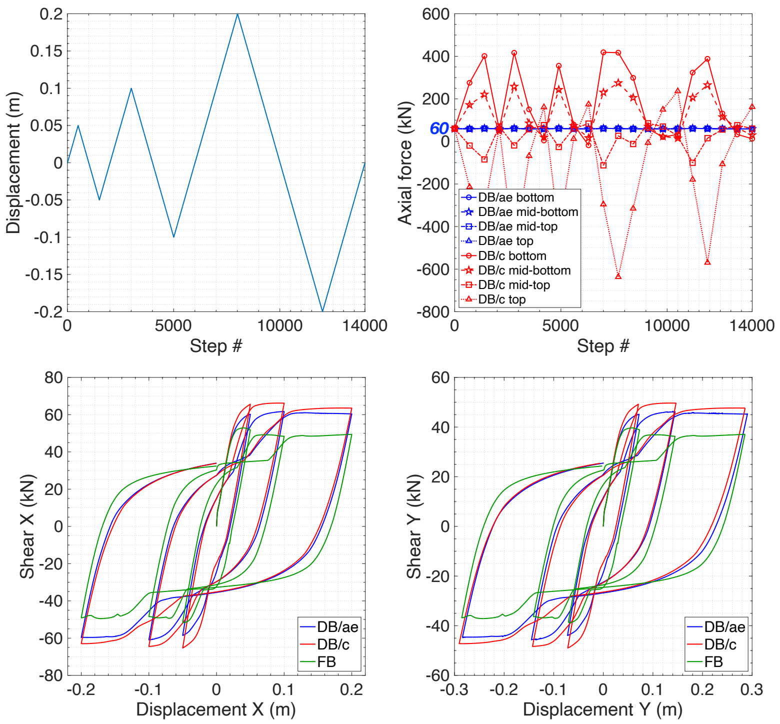

(a) (b)

Figure 3. (a,top) Cyclic displacement pattern applied along the cross-section diagonal. (b,top) Axial force estimates obtained with the DB/ae and DB/c formulations at the four IPs of the base element. Shear force-displacement curves for the DB/ae, DB/c and FB formulations, in the (a,bottom) x-direction and (b,bottom) y-direction.

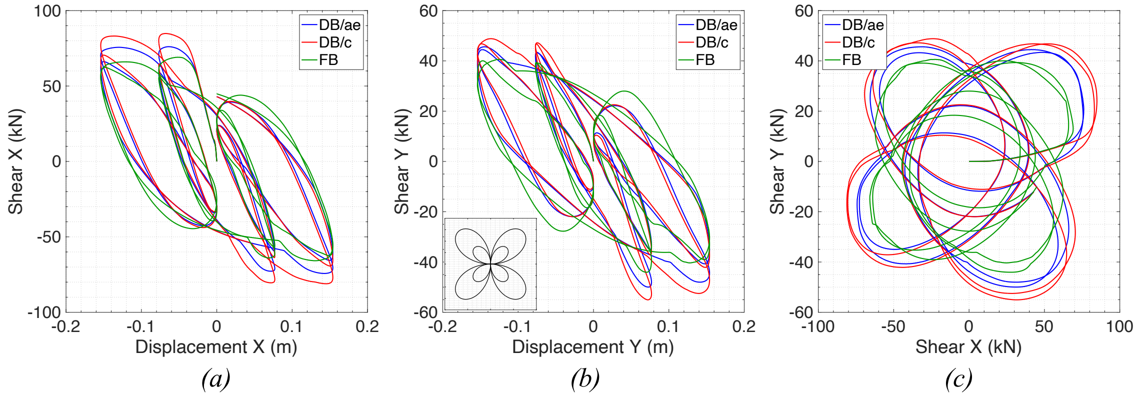

Figure 4. Response to cyclic clover leaf pattern: shear force-displacement curves for the DB/ae, DB/c and FB formulations, in the (a) x-direction and (b) y-direction, and (c) bidirectional shear force curve.

3 COMPARISON AGAINST BIDIRECTIONAL CYCLIC TESTING RESULTS

With a view to highlight the strengths and weaknesses of the proposed 3D DB/ae formulation with respect to the classical DB and FB formulations, the numerical responses from models employing all three types of element were compared against experimental testing results obtained from one series of experimental tests on RC thin walls, in terms of global (force-displacement) and local (curvature and axial force profiles) quantities.

In particular, the experimental campaign considered herein, described in the paper by Almeida *et al.* (2017), is the quasi-static bidirectional cyclic tests conducted on five thin T-shaped RC walls at the Earthquake Engineering and Structural Dynamics Laboratory (EESD Lab), École Polytechnique Fédérale de Lausanne (EPFL), Switzerland. Of the five specimens (called TW1 to TW5), only the last two test units (namely TW4 and TW5) are considered herein, being subjected to a combination of in-plane and out-of-plane loads.

Wall TW4, whose cross-section is depicted in Figure 5a), was 2000 mm tall, 80 mm thick, and 2700 mm long, with a lateral flange 80 mm thick and 440 mm wide. The longitudinal reinforcement layout consisted of a single layer with 11 ϕ6 bars (corresponding to a total reinforcement ratio of 0.72% in the web), three additional ϕ16 bars at each end boundary, and four ϕ6 bars along the short flange. The ϕ6 longitudinal bars had 350 mm long straight lap splices at the bottom of the wall, whilst the ϕ16 bars were continuous. The transverse reinforcement consisted of 10 ϕ6 bars at 200 mm spacing. Only the ground story of the idealised wall was actually constructed in the laboratory, and a shear span of 10 m, corresponding to a shear span ratio of 3.70, was simulated through several coupled servo-controlled actuators. The ϕ6 and ϕ16 bars were characterised by two different steel materials, having yield stress of 460 MPa and 515 MPa, ultimate stress of 625 MPa and 618 MPa, and ultimate strain of 9.9% and 12.7%, respectively. The concrete compressive strength was determined to be 31.2 MPa. The applied constant axial load ratio was 3.3%.

Wall TW5, whose cross-section is depicted in Figure 5b), was 2000 mm tall, 120 mm thick, and 2700 mm long, with a lateral flange 120 mm thick and 440 mm wide. The longitudinal reinforcement layout consisted of a double layer with a total of 66 ϕ6 bars, 54 of which in the web (corresponding to a reinforcement ratio of 0.49%) and the remaining 12 in the flange. The transverse reinforcement consisted of 30 ϕ6 bars at 130 mm spacing. In the southern boundary region, 15 U-shaped ϕ6 at 130 mm spacing were introduced. It is noted that the transversal bars, which should act as stirrups, were uncommonly placed on the inside of the longitudinal rebars, a detail representative of the reproduced construction practice that provides an unclear level of confinement to the concrete (Almeida *et al.*, 2017). The concrete cover was 15 mm. In the case of TW5, the shear span was set to 7.35. For the longitudinal and transverse ϕ6 bars, the same steel material characterising the ϕ6 bars in wall TW4 was used. The concrete compressive strength was determined to be 33.6 MPa. The applied constant axial load ratio was 4.8%. For both specimens, the loading protocol consisted of a reversed cyclic history, applied in displacement control in both horizontal directions and including a number of load stages, the latter corresponding to the peak (positive and negative) drift values. For more detailed information on the test setup, the reader is referred to the paper by Almeida *et al.* (2017).

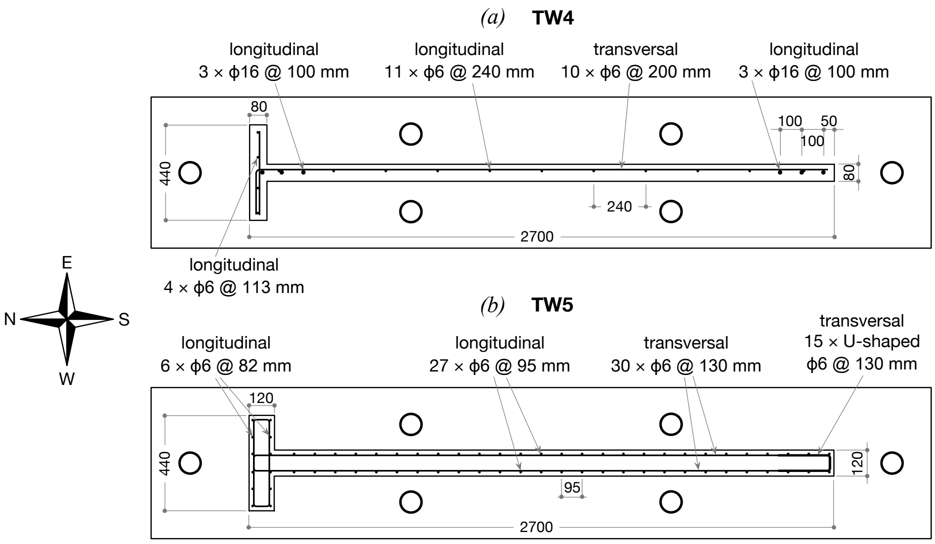

Figure 5. Cross-sectional layout of walls tested at EPFL: (a) TW4 and (b) TW5. All dimensions are in mm.

For the DB/ae and DB/c formulations, the wall model was discretised with two finite elements. The length of the base element was set to 0.6 m for TW4, so as to obtain the best match with the experimental results at the global level (see Figure 6). For TW5 three different bottom-length values, namely 0.2 m, 0.4 m and 0.6 m, were adopted to carry out a sensitivity analysis at the local level. On the other hand, only one element was employed for the FB formulation. All elements were assigned four Gauss-Lobatto integration sections. In the TW4 model, the lap splice of the ϕ6 longitudinal bars was not modelled, because the experimental observations showed not to overly influence the response (unlike with unit TW3, not addressed herein), and also due to epistemic uncertainty related to that modelling detail. Due to the presence of a single layer of bars, with no stirrups, concrete confinement was not modelled. In the TW5 model, due to the above-mentioned position of the transversal bars, concrete confinement was not modelled as well. Regarding the sectional discretisation, 130 and 22 fibres were adopted in both models for the longer sides of the web and the flange, respectively, whilst the shorter sides of both the web and the flange were represented with four and six fibres for TW4 and TW5, respectively.

Table 2. Parameter values adopted for concrete and steel in both TW4 and TW5 models.

<table>
<tr><th>Model</th><th>E_c (GPa)</th><th>f'_c (MPa)</th><th>ε_c (‰)</th><th>E_s (ϕ6) (GPa)</th><th>f_y (ϕ6) (MPa)</th><th>b (ϕ6) (%)</th><th>E_s (ϕ16) (GPa)</th><th>f_y (ϕ16) (MPa)</th><th>b (ϕ16) (%)</th></tr>
<tr><td>TW4</td><td>29.2</td><td>31.2</td><td>2.1</td><td rowspan="2">184</td><td rowspan="2">460</td><td rowspan="2">0.93</td><td>210</td><td>515</td><td>0.4</td></tr>
<tr><td>TW5</td><td>31.7</td><td>33.6</td><td>2.1</td><td>-</td><td>-</td><td>-</td></tr>
</table>

A linear geometric transformation was adopted (geometric nonlinearities not included), since the experimentally imposed loading, in terms of ratio between the moment applied by the actuators at the top of the walls and the horizontal load, was based on a geometrically linear relation. The Concrete04 material model was used for concrete, whilst the Steel02 material model was assigned to the longitudinal (both ϕ6 and ϕ16 bars) and transverse reinforcement. All the adopted parameter values are reported in Table 2. Given these material and sectional properties, the torsional rigidity resulted to be $GJ = 5078$ kNm^2 and $GJ = 18430$ kNm^2, for TW4 and TW5, respectively.

As for the previous numerical cases, a dynamic analysis framework with two single-point constraints was employed to apply the displacement path to the models. To correctly reproduce the shear span of the specimens, in both wall models an additional node was created at the height of 10 m and 7.35 m for walls TW4 and TW5 respectively, where the bidirectional displacement path was then applied. Such a node was linked by a rigid elastic element to the nonlinear portion of the model, made of one or two elements depending on the formulation. Consequently, it was required to multiply the displacement patterns along the two directions by two constant scaling factors, which were iteratively adapted until a good match was obtained between the bidirectional target pattern (i.e. the one imposed in the tests) and the pattern actually recorded at the top node of the nonlinear portion of the model, at a 2 m height. In order to reflect the loading conditions of the tests and to avoid giving rise to unwanted moments, the vertical load was instead applied at the top node of the nonlinear portion of the model.

As far as the global level is concerned, Figure 6 displays, for both walls TW4 and TW5, the comparisons between the experimental in-plane shear-displacement curves and the numerical ones, obtained adopting the three formulations that are investigated in this work. The length of the base element for the two DB formulations within the TW5 model was set to 0.6 m for consistency with the value adopted in the TW4 model; by comparison with the curves related to the other two values considered herein, namely 0.2 m and 0.4 m, it was observed that the obtained curves are all similar, meaning that the base element's length does not play an important role at the global level, as expected. It can be noted for both walls that i) the three types of element lead to curves that are almost superimposed, and ii) the agreement with the experimental curves is poor, which was anticipated. In fact, the plane-sections-remaining-plane assumption is not adequate for long cross-sections as it does not capture the nonlinear strain profile developing along the wall length, even for flexurally governed walls with relatively high shear span ratios (Almeida *et al.*, 2016).

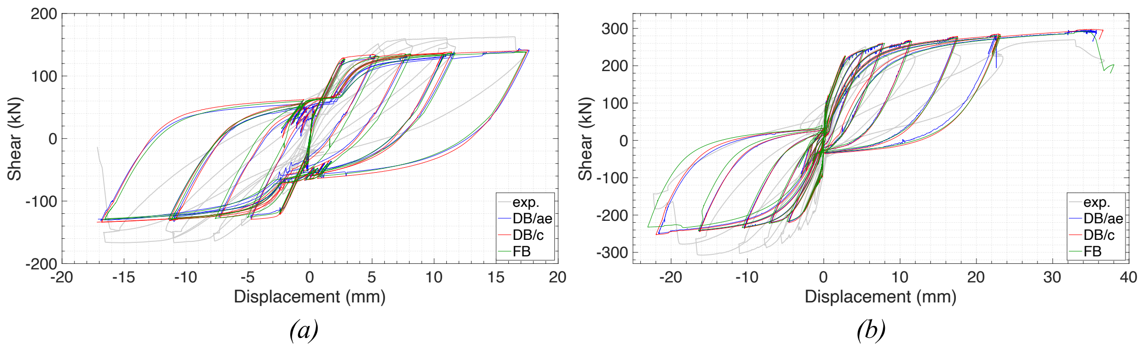

Figure 6. Experimental in-plane shear force-displacement curves, and numerical results obtained with the DB/ae, DB/c and FB formulations, for (a) TW4 and (b) TW5.

Focusing now on the local level, only the two DB formulations for wall TW5 are considered for comparison, given that the aim of this work is exploring the benefit of the axially equilibrated formulation with respect to its classical counterpart. In Figure 7a), the axial forces obtained in all IPs of the two elements discretising the wall, for both the DB/ae and DB/c formulations, are compared against the experimental (constant) axial force profile. The numerical profiles related to the three different lengths of the base element are superimposed and shown with the same colour, for each of the two DB formulations. The plot clearly confirms what was already shown in Figure 3b,top) above, that is, the use of classical displacement-based elements yields different values of axial force at distinct IPs, whilst the 3D DB/ae formulation leads the axial force in the four IPs of the two elements to be constant and very similar to the external applied axial load. The in-plane curvature profiles obtained with the two DB formulations, again for different lengths of the base element, are compared against the experimental profile in Figure 7b). It can be readily observed how the multi-linear curvature profile exhibited by the DB/ae formulation is smoother than the one provided by the DB/c approach, which tends to be piece-wise vertical with sharper discontinuities between adjoining elements. Such advantageous feature of DB/ae reflects on a less scattered simulation of the base curvature for the three meshes, which unsurprisingly also better reproduces experimental measurements. Incidentally, it is noted that the best experimental vs. numerical match is obtained when the base element's length is set to 0.2 m, capturing the concentration of deformation in the plastic zone at the wall base. The above aspects described for in-plane curvature are also apparent for the out-of-plane curvature profiles, shown in Figure 7c) for both DB formulations. Here the slope of the curvature exhibited by the two DB/c elements results to be increased with respect to the in-plane case, though in any case considerably less smooth than that produced by the DB/ae formulation, which is deemed more in line with the real test, especially considering the very small thickness of the wall.

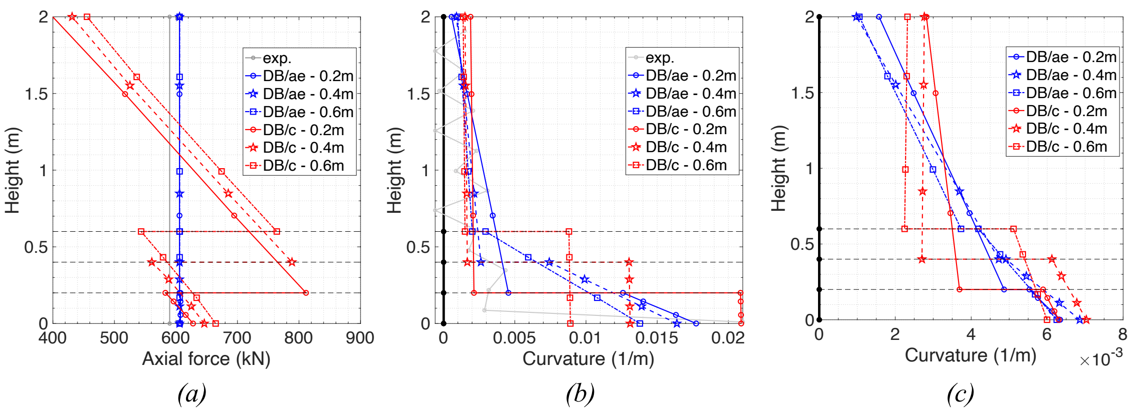

Figure 7. Wall TW5: experimental results and numerical output obtained with the DB/ae and DB/c formulations, for different lengths of the base element: (a) (constant) axial force profile, (b) in-plane curvature profiles, (c) out-of-plane curvature profiles.

Still on the local level, the two DB formulations were also compared in terms of stress-strain curves for several steel fibres at the base integration section, with reference to the TW5 wall model with a base element's length of 0.2 m. For most of the rebars, the curves (not shown here due to space constraints) show a reasonable agreement, whereas they diverge substantially for the South rebar, especially concerning the most intense compression cycle; this is expected, given that the South side of the cross-section, being just 120 mm thick, is subjected to a (compression) stress-strain field that is more intense than in the North side (where the flange is located). The significantly different maximum compressive strains – which could be used for seismic design or assessment verifications – obtained by the two approaches are ultimately a consequence of the lack of strict axial equilibrium of DB/c, further highlighting the importance of developing formulations that avert numerical pathologies, such as the current DB/ae.

4 CONCLUSIONS

Although the classical displacement-based formulation (DB/c) shows advantageous features in simulating tension shift effects in structural members, it does not verify full equilibrium in the axial member direction. Several authors recently proposed enhanced strain formulations for 2D beams that bypass this drawback. This work presented the implementation in OpenSees of the extension to 3D (see Cavalieri *et al.*, 2022) of a recently developed axially equilibrated DB (DB/ae) planar beam element. The numerical performance of the new beam element was compared with those obtained with the DB/c and FB elements, firstly considering an example column subjected to monotonic and cyclic bidirectional loading, and then using experimental results from one series of quasi-static bidirectional cyclic tests on two RC thin walls as benchmark.

It could be gathered that at the global level the performances of DB/c and DB/ae are quite similar. On the other hand, significant divergencies were observed at the local level. In particular, it was confirmed that DB/c elements ensure axial equilibrium only in an average sense and yield different values of axial force at distinct IPs, whilst the spatial DB/ae formulation leads the axial force in all integration points to be constant and coincident with the external applied axial load. Consequently, the DB/ae formulation exhibits a multi-linear curvature profile that better reproduces experimental measurements. All these observations provide reassurance on the increased accuracy of the proposed 3D DB/ae formulation and highlight the need to develop formulations that avert numerical pathologies.

REFERENCES

Almeida J.P., Prodan O., Rosso A. and Beyer K. (2017). Tests on thin reinforced concrete walls subjected to in-plane and out-of-plane cyclic loading. *Earthquake Spectra*, V.33, No.1, 323-345.

Almeida J.P., Tarquini, D. and Beyer K. (2016). Modelling approaches for inelastic behaviour of RC walls: multi-level assessment and dependability of results. *Archives of Computational Methods in Engineering*, V.23, No.1, 69-100.

Cavalieri F., Calò M., Almeida J.P. and Pinho R. (2022). Spatial nonlinear displacement-based beam element with enhanced strains for axial equilibrium. *Earthquake Engineering & Structural Dynamics* (submitted).

McKenna F., Fenves G.L., Scott M.H. and Jeremic B. (2000). *OpenSees: Open system for earthquake engineering simulation*. Pacific Earthquake Engineering Research Center, University of California, Berkeley, USA. Available at: http://opensees.berkeley.edu. [Last accessed 27 May 2022].

Menegotto M. and Pinto P.E. (1973). Method of analysis for cyclically loaded RC plane frames including changes in geometry and non-elastic behaviour of elements under combined normal force and bending. In *Proceedings of Symposium on the Resistance and Ultimate Deformability of Structures Acted on by Well Defined Repeated Loads, International Association for Bridge and Structural Engineering*, Zurich, Switzerland, pp. 15-22.

Popovics S. (1973). A numerical approach to the complete stress–strain curve of concrete. *Cement and Concrete Research*, V.3, No.5, 583-599.

Raza S., Menegon S.J., Tsang H.H. and Wilson J.L. (2020). Force-displacement behavior of limited ductile high-strength RC columns under bidirectional earthquake actions. *Engineering Structures*, V.208, 110278.

Rodrigues H., Arêde A., Varum H. and Costa A.G. (2013). Experimental evaluation of rectangular reinforced concrete column behaviour under biaxial cyclic loading. *Earthquake Engineering & Structural Dynamics*, V.42, No.2, 239-259.

Takizawa H. and Aoyama M. (1976). Biaxial effects in modelling earthquake response of RC structures. *Earthquake Engineering & Structural Dynamics*, V.4, No.6, 523-552.

Tarquini D., Almeida J.P. and Beyer K. (2017). Axially equilibrated displacement-based beam element for simulating the cyclic inelastic behaviour of RC members. *Earthquake Engineering & Structural Dynamics*, V.46, No.9, 1471-1492.